OXFORD

Journal of Geophysics and Engineering

Journal of Geophysics and Engineering (2021) **18**, 712–724 https://doi.org/10.1093/jge/gxab047

The mechanical responses in monopole acoustic LWD and their relation with the output voltage waveform

Chao Zhang, Da Chen and Hengshan Hu*

Department of Astronautics and Mechanics, Harbin Institute of Technology, Harbin 150001, China

*Corresponding author: Hengshan Hu. E-mail: hhs@hit.edu.cn

Received 20 July 2021, revised 5 August 2021
Accepted for publication 20 August 2021

Abstract

Acoustic logging while drilling (LWD), characterised by simultaneous drilling and logging, is widely used to obtain the elastic parameters of the formation around the borehole. Most published monopole acoustic LWD simulation waveforms are routinely presented as pressure. However, these pressure waveforms disagree with the voltage waveforms recorded in the experiments. Here, to find out the reason of the inconsistent of these two waveforms, both the piezoelectric effect of the transducer and the propagation of the acoustic wave are integrally calculated with the finite-element method, obtaining the voltage waveform as well as the mechanical waveforms. The quantitative comparisons between the mechanical waveforms and the voltage waveform show that the output voltage cannot represent the pressure signal, but a combination of multiple mechanical signals. Based on the piezoelectric equation and the structure of the piezoelectric transducer used in this paper, we formulate the output voltage in terms of the four mechanical quantities, i.e. the radial strain and axial stress of the transducer as well as the acoustic pressure and the radial displacement of the borehole fluid. Furthermore, the contributions of these four mechanical quantities to different wave groups are explored. Finally, the waveforms comparisons after drill collar grooving reveal that the displacement waveform before and after grooving should also be displayed when evaluating the grooving effect instead of only the pressure waveform as in previous studies.

Keywords: acoustic logging while drilling (LWD), boundary condition, finite-element method (FEM), piezoelectric effect, voltage

1. Introduction

Different from wireline logging, the logging while drilling (LWD) technique performs drilling and logging simultaneously. The LWD costs less time, measures the formation before mud invasion, and makes it possible to guide the drilling direction. Hence LWD has received increasing attention from exploration geophysicists in recent decades. Experimental measurement and theoretical simulation are two common and important ways to understand the propagation mechanisms of acoustic waves in the acoustic LWD.

Few experiments have been conducted in laboratory for acoustic LWD. Zhu *et al.* (2008) conducted acoustic LWD experiments with a scaled acoustic logging tool in isotropic and anisotropic borehole models. Wang *et al.* (2016) analysed the propagation characteristics of collar waves excited by multipole sources. Wang *et al.* (2017) compared acoustic and seismoelectric LWD and studied the propagation characteristics of collar waves and seismoelectric waves. It can be noted that the waveforms in their experiments contain a strong collar wave and a weak Stoneley wave in monopole acoustic LWD.

A lot of theoretical simulations have been carried out for acoustic LWD. Tang *et al.* (2002) calculated synthetic full waveforms and velocity dispersion curves in monopole acoustic LWD. Cui (2004) calculated full waveforms and dispersion curves in elastic and porous formations. Sinha *et al.* (2009) calculated radial variations of displacement and pressure amplitudes, and emphasised 'the importance of exposing transducer to the borehole fluid through a slotted pipe'. Wang *et al.* (2013) studied the acoustic reflection wave fields in monopole LWD by using the finite difference and finite-element methods. Su *et al.* (2015) suggested that a collar sound insulator could be made by using the stop bands of a collar with different thicknesses in monopole LWD. Wang *et al.* (2016) proposed that the velocities of formation could be more easily measured with a composite material collar of high P velocity, S velocity and density. Zheng (2017) theoretically calculated individual waves in acoustic LWD and analysed their propagation characteristics. Yang *et al.* (2017) studied the effects of collar grooves on weakening the interference with formation waves. Fang and Cheng (2017) considered that the transmitted S-wave in slow formation could be used to obtain the formation S-wave velocity by 2D staggered-grid FDM. All these authors show only the acoustic pressure when studying the characteristics of waveforms. It can be noted that the synthesised waveforms expressed by pressure contain a weak collar wave and a strong Stoneley wave in monopole acoustic LWD, which are different from the waveforms recorded in the published experiments' results.

He *et al.* (2017) were the first to notice this phenomenon that 'the simulated collar waves are far weaker than those we encountered in the field data' in the published literature. They analysed the dependence of the pressure waveform on the depth of the transducer into a drill collar. When the transducer is shallowly indented into the collar, the calculated pressure waveform has a much smaller collar wave than that in the experiment. They then put the transducer deeper into the collar so that the collar wave became stronger and looked like that in the experiment. There may be tools that put the transducer deeper into the drill collar, but to our knowledge, in the commonly used tools, the transducers are 'slightly indented from the external surface of the tool housing' as pointed out in the patent (Wisniewski *et al.* 2003). The transducers are similarly described in another patent (Birchak *et al.* 1997). Therefore, the large discrepancies between the synthesised waveform and the experiment waveform remain to be explained for the transducer placed in the way as in patent by Wisniewski *et al.* (2003).

In this study, we calculate the voltage waveforms as well as acoustic waveforms by using the finite-element method that integrally considers both the piezoelectric effect of the transducer and the propagation of the acoustic wave, called the FEM-PP method. The paper is organised as follows. First, the voltage waveforms are qualitatively compared, respectively, with the waveforms of the pressure and the radial displacement in the fluid at the receiver position. Second, the similarities of the waveforms are quantitatively calculated between various mechanical quantities and voltage. Third, based on the piezoelectric equation, we formulate the output voltage in terms of the four mechanical quantities, i.e. the radial strain and axial stress of the transducer as well as the pressure and the radial displacement of the borehole fluid. Finally, we calculate the response after collar grooving.

2. Methodology

2.1. *Conventional method with piezoelectric effect ignored*

The commonly analytical method used by scholars for LWD waves does not consider the piezoelectric effect. The acoustic full waveforms are calculated by using the real axis integral (RAI) method and the acoustic individual waveforms are calculated by using the residue theorem and branch-cut integral. Since pressure and radial displacement are continuous at an interface, people pay attention to the two mechanical quantities.

The full-wave expressions of the pressure and the radial displacement (Cui 2004; Zheng 2017) are, respectively,

$$p(t,z,r)=\frac{1}{4\pi^2}\rho_f\int_{-\infty}^{\infty}\omega^2\int_{-\infty}^{\infty}\left[\frac{N_8(k_z,\omega)}{D(k_z,\omega)}I_n(\eta_f r)+\frac{N_9(k_z,\omega)}{D(k_z,\omega)}K_n(\eta_f r)\right]e^{ik_z z}dk_z e^{-i\omega t}d\omega, \quad (1)$$

and

$$u_r(t,z,r)=\frac{1}{4\pi^2}\rho_f\int_{-\infty}^{\infty}\omega^2\int_{-\infty}^{\infty}\left[\frac{N_8(k_z,\omega)}{D(k_z,\omega)}\left(\frac{n}{r}I_n(\eta_f r)+\eta_f I_{n+1}(\eta_f r)\right)+\frac{N_9(k_z,\omega)}{D(k_z,\omega)}\left(\frac{n}{r}K_n(\eta_f r)-\eta_f K_{n+1}(\eta_f r)\right)\right]e^{ik_z z}dk_z e^{-i\omega t}d\omega. \quad (2)$$

The individual-wave expressions of these two physical quantities (Zheng 2017) are, respectively,

$$p(t,z,r)=\frac{1}{2\pi}\int_{-\infty}^{\infty}p_0\rho_f\omega^2 S(\omega)\left\{ie^{ik_z z}U(k_z)\times\left[\frac{N_8(k_z,\omega)}{\partial D(k_z,\omega)/\partial k_z}I_n(\eta_f r)+\frac{N_9(k_z,\omega)}{\partial D(k_z,\omega)/\partial k_z}K_n(\eta_f r)\right]\right\}\Bigg|_{k_z=k_{pole}(\omega)}e^{-i\omega t}d\omega, \quad (3)$$

and

$$u_r(t,z,r) = \frac{1}{2\pi}\int_{-\infty}^{\infty} p_0\rho_f\omega^2 S(\omega)\left\{ ie^{ik_z z}U(k_z)\right.$$
$$\times\left[\frac{N_8(k_z,\omega)}{\partial D(k_z,\omega)/\partial k_z}\left(\frac{n}{r}I_n(\eta_f r)\right.\right.$$
$$\left.+\eta_f I_{n+1}(\eta_f r)\right) + \frac{N_9(k_z,\omega)}{\partial D(k_z,\omega)/\partial k_z}$$
$$\left.\left.\times\left(\frac{n}{r}K_n(\eta_f r) - \eta_f K_{n+1}(\eta_f r)\right)\right]\right\}\Bigg|_{k_z=k_{pole}(\omega)}$$
$$\times e^{-i\omega t}d\omega, \quad (4)$$

where r and z are the radial and axial distances between the receiver and the source; ω denotes the angular frequency; t denotes the time; ρ_f denotes the fluid density; v_f is the fluid acoustic velocity; $k_f = \omega/v_f$ denotes the wavenumber in the fluid; k_z denotes the axial wavenumber; $\eta_f = (k_z{}^2 - k_f{}^2)^{1/2}$ denotes the radial wavenumber in the fluid; k_{pole} is the pole associated with an individual wave; $K_n(x)$ and $I_n(x)$ are the first kind and second kind modified Bessel function of order n ($n = 0$ for monopole), respectively; $D(k_z,\omega)$ is the determinant of the coefficient matrix of the acoustic field, which depends on the frequency, wavenumber and the geometric characteristics of the media inside and outside the borehole, and its zero point is the pole of the acoustic field function; $N_8(k_z,\omega)$, $N_9(k_z,\omega)$ are, respectively, the values of the determinant of the matrix obtained by replacing the columns 8 and 9 of the acoustic field coefficient matrix to the acoustic source vector and p_0 is the magnitude of the pressure source. The frequency spectrum $S(\omega)$ and the wavenumber spectrum $U(k_z)$ of the pressure source are

$$\mathrm{S}(\omega) = \mathrm{FT}[\mathrm{f}(t)], \quad (5)$$

and

$$\mathrm{U}(k_z) = \mathrm{FT}[\mathrm{Z}(z)], \quad (6)$$

where $\mathrm{FT}(\cdot)$ is the Fourier transform operator. The pressure source p^s varies over time and space as follows (Zheng 2017)

$$p^s(t,z) = p_0 \mathrm{f}(t)\,\mathrm{Z}(z), \quad (7)$$

with

$$\mathrm{f}(t) = \begin{cases} \frac{1}{2}\left[1+\cos\frac{2\pi}{T_c}\left(t-\frac{T_c}{2}\right)\right]\cos 2\pi f_0\left(t-\frac{T_c}{2}\right), & 0 \le t \le T_c \\ 0. & t<0 \text{ or } t>T_c \end{cases}, \quad (8)$$

and

$$\mathrm{Z}(z) = \begin{cases} \cos\frac{\pi}{2z_0}z, & -z_0 \le z \le z_0 \\ 0, & z<-z_0, z>z_0 \end{cases}, \quad (9)$$

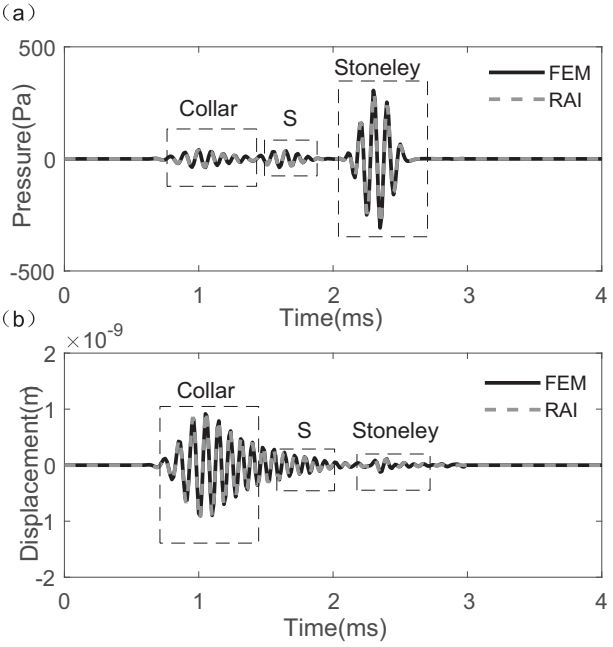

Figure 1. Comparisons of (a) pressure and (b) radial displacement waveforms between the FEM and RAI methods. The dashed gray lines show the pressure and radial displacement waveforms with the center frequency of 10 kHz calculated by the RAI method described in equation (1) of the full-wave expression of the pressure, and equation (2) of the full-wave expression of the radial displacement. The black lines show the pressure and radial displacement waveform calculated by the FEM without considering the piezoelectric effect, with the same pressure source and receiving position as the RAI method.

where $2z_0$ is the height of the acoustic source; $\mathrm{f}(t)$ is a cosine envelope pulse (Zhang *et al.* 1994) of the duration T_c and the center frequency f_0 and $\mathrm{Z}(z)$ is an axially varying cosine function of period $4z_0$.

The FEM without considering the piezoelectric effect is also commonly used by scholars to study LWD (Wang *et al.* 2013; Matuszyk *et al.* 2014). To verify its accuracy, we compared it with the RAI method in figure 1.

As shown in the dashed gray lines in figure 1, the pressure and radial displacement waveforms with the center frequency of 10 kHz are calculated by the RAI method described in equation (1) of the full-wave expression of the pressure, and equation (2) of the full-wave expression of the radial displacement. On the contrary to the pressure waveform with a weak collar wave and a strong Stoneley wave, the radial displacement waveform contains a strong collar and a weak Stoneley wave, which is consistent with the characteristics of the experimental waveform (Zhu *et al.* 2008; Wang *et al.* 2016). The black lines in figure 1 show the pressure and radial displacement waveform calculated by the FEM without considering the piezoelectric effect, with the same pressure source and receiving position as the RAI method. The pressure waveforms calculated by the two methods are almost indistinguishable in figure 1a, and the radial displacement waveforms are the same in figure 1b.

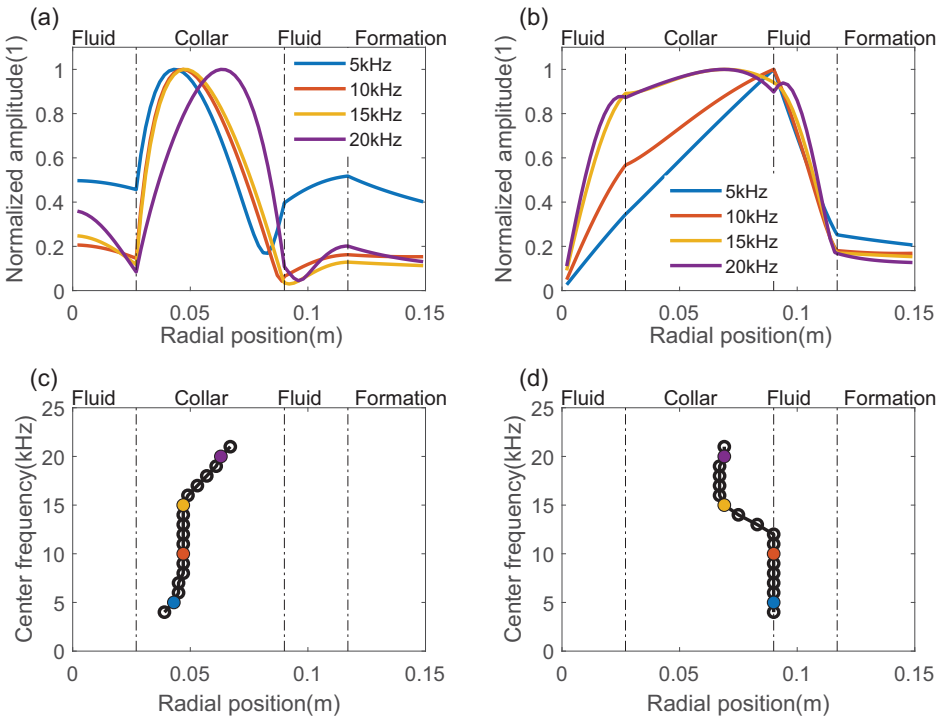

Figure 2. The normalised (a) pressure and (b) radial displacement of the collar wave plotted as a function of the radial position at different center frequencies (5, 10, 15 and 20 kHz). The radial position corresponding to the maximum amplitude of the normalised (c) pressure and (d) radial displacement of the collar wave at different frequencies. For example, the blue line in (a) with the center frequency of 5 kHz and the radial position of 0.043 m corresponding to maximum amplitude is mapped to the blue point with the same center frequency and radial position in (c). Part (c) provides the calculation results at more different center frequencies than (a). Parts (b) and (d) are mapped in the same way.

The collar waves of the pressure and the radial displacement are calculated by summing the residuals of corresponding poles (Zheng 2017; Ji *et al.* 2019) as equations (3) and (4) at different radial positions and at a 3-m axial position from the source. The normalised pressure and radial displacement of the collar wave are plotted as a function of the radial position at different center frequencies (5, 10, 15 and 20 kHz) in figure 2a and b. Figure 2 parts c and d show the radial position corresponding to the maximum amplitude of the normalised pressure and radial displacement of the collar wave at different frequencies. For example, the blue line in figure 2a with the center frequency of 5 kHz and the radial position of 0.043 m corresponding to maximum amplitude is mapped to the blue point with the same center frequency and radial position in figure 2c. Figure 2c provides the calculation results at more different center frequencies than figure 2a. Figure 2 parts b and d are mapped in the same way. Figure 2 parts a and c show that the energy of the collar wave in pressure waveform is mainly concentrated in the inner wall of the collar at low frequency, and gradually moves outwards with the increase in frequency. On the contrary, figure 2 parts b and d show that the energy of collar wave in displacement waveform is mainly concentrated in the outer wall of the collar at low frequency, and gradually moves inwards as the frequency increases after the critical value of 12 kHz in this model.

These two types of waveform show the opposite characteristics in the radial distribution of the collar wave energy, which causes confusion in the choice of which grooving method (internal or external grooving) to use to weaken the collar wave. Therefore, it is of significance to determine which signal is closer to the voltage signal recorded by the transducer. A good idea is to compare these two mechanical quantities with the voltage signal recorded by the transducer, which motivates us to build the following FEM model taking the piezoelectric effect into account.

2.2. *FEM-PP method with the piezoelectric effect considered*

To clarify the relations between the mechanical quantities and the voltage received by the transducer, we establish a FEM model considering both the piezoelectric effect of the transducer and the propagation of the acoustic wave, hence called the FEM-PP method, by using finite-element solver COMSOL Multiphysics®. In this way, the piezoelectric effect is taken as an integral part of the whole process from voltage

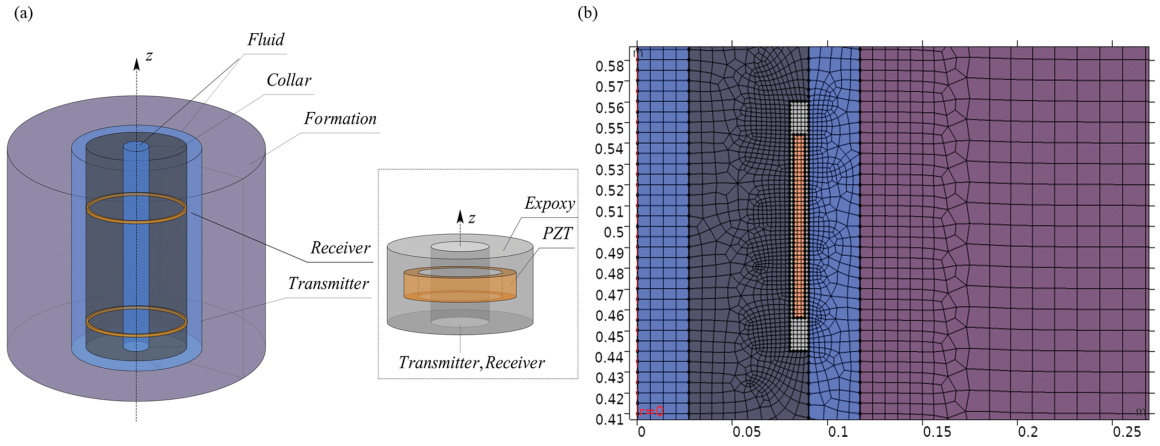

Figure 3. The (a) schematic and the (b) spatial grid assignment of the acoustic LWD model with the fluid, the collar, the formation and the transducers. In the radial direction, the model can be decomposed into four portions, i.e. the fluid inside the collar, the collar, the fluid outside the collar and the formation. The acoustic LWD tool consists of a transmitting transducer and a receiving transducer separated by 3 m. The two transducers, with the same geometric structure surround by the epoxy seal, are shallowly embedded in the outer surface of the collar.

signal generation to acoustic wave propagation and then to voltage signal reception.

The three-dimensional axisymmetric geometry configuration of the FEM model is shown in figure 3a. In the radial direction, the model can be decomposed into four portions, i.e. the fluid inside the collar, the collar, the fluid outside the collar and the formation. The acoustic LWD tool consists of a transmitting transducer and a receiving transducer separated by 3 m. The two transducers, with the same geometric structure surround by the epoxy seal, are shallowly embedded in the outer surface of the drill collar (Wisniewski *et al.* 2003). The two tubular piezoelectric transducers are polarised in the radial direction. The inner wall of the piezoelectric ceramic tube is grounded, and the outer wall is connected with excitation voltage expressed by the cosine envelope impulse in equation (8).

In FEM, the fluid–solid boundary conditions and solid–solid boundary conditions of the axisymmetric model are, respectively, stipulated by

$$\begin{cases} u_r{}^s = u_r{}^f \\ \sigma_{rr}{}^s = -p^f \\ \sigma_{rz}{}^s = 0 \\ \sigma_{r\theta}{}^s = 0 \end{cases}, \tag{10}$$

and

$$\begin{cases} u_r{}^{s1} = u_r{}^{s2} \\ u_\theta{}^{s1} = u_\theta{}^{s2} = 0 \\ u_z{}^{s1} = u_z{}^{s2} \\ \sigma_{rr}{}^{s1} = \sigma_{rr}{}^{s2} \\ \sigma_{r\theta}{}^{s1} = \sigma_{r\theta}{}^{s2} = 0 \\ \sigma_{rz}{}^{s1} = \sigma_{rz}{}^{s2} \end{cases}, \tag{11}$$

where the superscripts f and s refer to fluid and solid on either side of the boundary; Subscripts $s1$ and $s2$ refer to two different solids on either side of the boundary.

In this multiphysics field coupling model, we simulate the acoustic field in borehole fluid, elastic field in the solid and the coupling mechanical and electrostatics field in the piezoelectric ceramic tube. Far field boundaries of the fluid and the solid are set as a plane-wave-radiation boundary (Givoli & Neta 2004) and low-reflecting boundary (Lalanne & Touratier 2000), respectively, to reduce the interference of reflected waves at the boundary. As shown in figure 3b, the mesh type is free quadrilateral with the maximum size of $v/(6f_0)$, where v is the minimum velocity of all the materials in the model and f_0 is the center frequency of excitation voltage. Model parameters and material parameters are shown in Tables 1 and 2.

Figure 4 shows the process of excitation, propagation and reception of acoustic waves simulated by the FEM-PP method. The transmitter converts the input voltage V signal into various mechanical signals, such as, strain ε, stress σ, displacement **u**, particle velocity **v**, and particle acceleration **a** through an inverse-piezoelectric effect. After the acoustic waves propagate to the receiver, the receiver converts those mechanical quantities back to the voltage V through piezoelectric effect.

Based on the FEM-PP method, we obtain the wave field snapshot of radial displacement and pressure (negative radial stress) at 1.4 ms with 10 kHz of the excitation voltage. Figure 5 shows three wave groups, namely collar wave, shear wave, and Stoneley wave in order of velocity from fast to slow, the same as the wave group type and the wave group number in figure 1. In the following, the relationships between voltage waveforms and mechanical waveforms are explored, and the numerical results are all calculated by the FEM-PP method proposed in this section.

Table 1. Materials and geometric parameters of fluid, drill collar, piezoelectric transducer and formation

Component	Density ($kg\,m^{-3}$)	P-wave velocity ($m\,s^{-1}$)	S-wave velocity ($m\,s^{-1}$)	Thickness (m)	Height (m)
Inner fluid	1000	1470	-	0.027	$+\infty$
Drill collar	7800	5860	3131	0.063	$+\infty$
Piezoelectric Ceramics (PZT-5H)	7500	4118	1751 (SV) 1770 (SH)	0.006	0.088
Epoxy	1500	3089	1589	0.010	0.120
Outer fluid	1000	1470	-	0.027	$+\infty$
Formation	2320	3970	2455	$+\infty$	$+\infty$

Table 2. Elastic, piezoelectric and relative dielectric constant of PZT-5H

Elastic constant (1/Pa)		Piezoelectric constant (C/N)	Relative dielectric constant (1)
$s_{11} = s_{22} = 1.65e\text{-}11$	$s_{33} = 2.07e\text{-}11$	$d_{15} = d_{24} = 7.41e\text{-}10$	
$s_{12} = s_{21} - 4.78e\text{-}12$	$s_{44} = s_{55} = 4.35e\text{-}11$	$d_{31} = d_{32} - 2.74e\text{-}10$	$\varepsilon_{11} = \varepsilon_{22} = 3130$
$s_{13} = s_{31} = s_{23} = s_{32} - 8.45e\text{-}12$	$s_{66} = 4.26e\text{-}11$	$d_{33} = 5.93e\text{-}10$	$\varepsilon_{33} = 3400$

Note that the other elements not specified in the table are all zero.

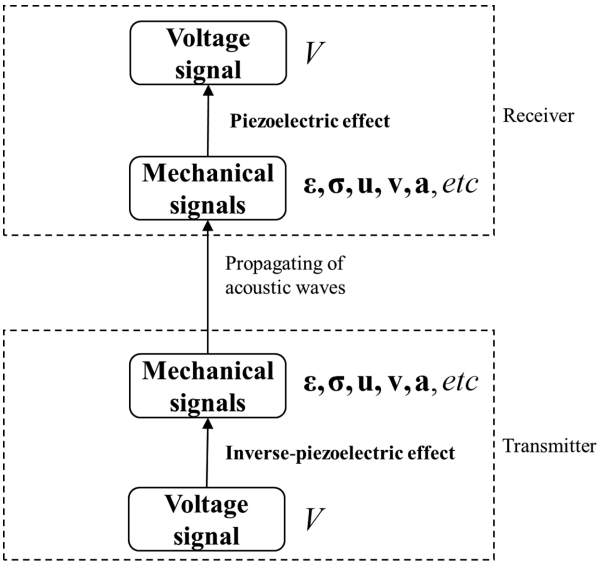

Figure 4. The process of excitation, propagation and reception of acoustic waves simulated by the FEM-PP method.

3. Numerical examples

3.1. *Waveform difference of voltage from pressure and radial displacement*

In section 2, we proposed the FEM-PP method considering both the piezoelectric effect of the transducer and the propagation of the acoustic wave. In this section, the waveforms of the pressure, the radial displacement, and the voltage are calculated by the FEM-PP method. Their differences and similarities are explored by establishing three models as the follows.

(i) In model 1 as shown in figure 6a, the tube transducer is slightly indented from the external surface of the collar with the thickness of 0.063 m and the collar is placed in the infinite fluid;
(ii) In model 2 as shown in figure 6b, the tube transducer is slightly indented from the external surface of the collar with the thickness of 0.063 m and the collar is placed in the borehole;
(iii) In model 3 as shown in figure 6c, the tube transducer is slightly indented from the external surface of the collar with the thickness of 0.050 m and the collar is placed in the borehole.

The voltage source applied to the transmitting transducer is a cosine envelope pulse with a center frequency of 10 kHz. The normalised waveforms of voltage, radial stress (negative pressure) and radial displacement are calculated at the outer surface center of the receiver. Figure 6 shows the schematic diagrams of these three models and the corresponding normalised waveforms. Each waveform has two distinct waves, which are the collar wave and Stoneley wave in order of arrival time. In the three FEM models, voltage waveforms show the similar characteristic with a strong collar wave and a weak Stoneley wave, which is consistent with the characteristics of the voltage waveform recorded in the experiments (Zhu *et al.* 2008; Wang *et al.* 2016).

As in figure 6d, when the collar is placed in the infinite fluid, the pressure and radial displacement waveforms both have a strong collar wave and a weak Stoneley wave, which is similar to the characteristic of voltage waveforms. As in figure 6e, when the collar is placed in the borehole, the radial displacement waveform has a strong collar wave and a weak

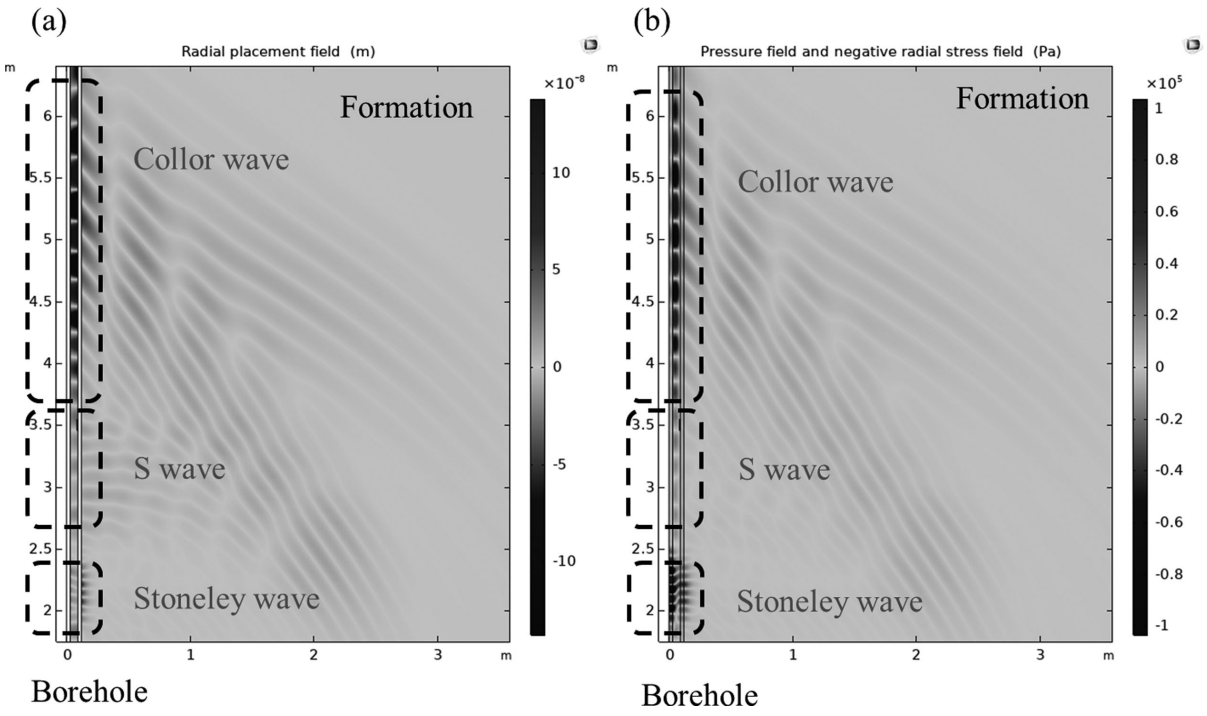

Figure 5. Acoustic wave field snapshot of (a) radial displacement and (b) pressure (negative radial stress) at 1.4 ms with 10 kHz of the excitation voltage. There are three wave groups; namely the collar wave, shear wave and Stoneley wave in order of velocity from fast to slow.

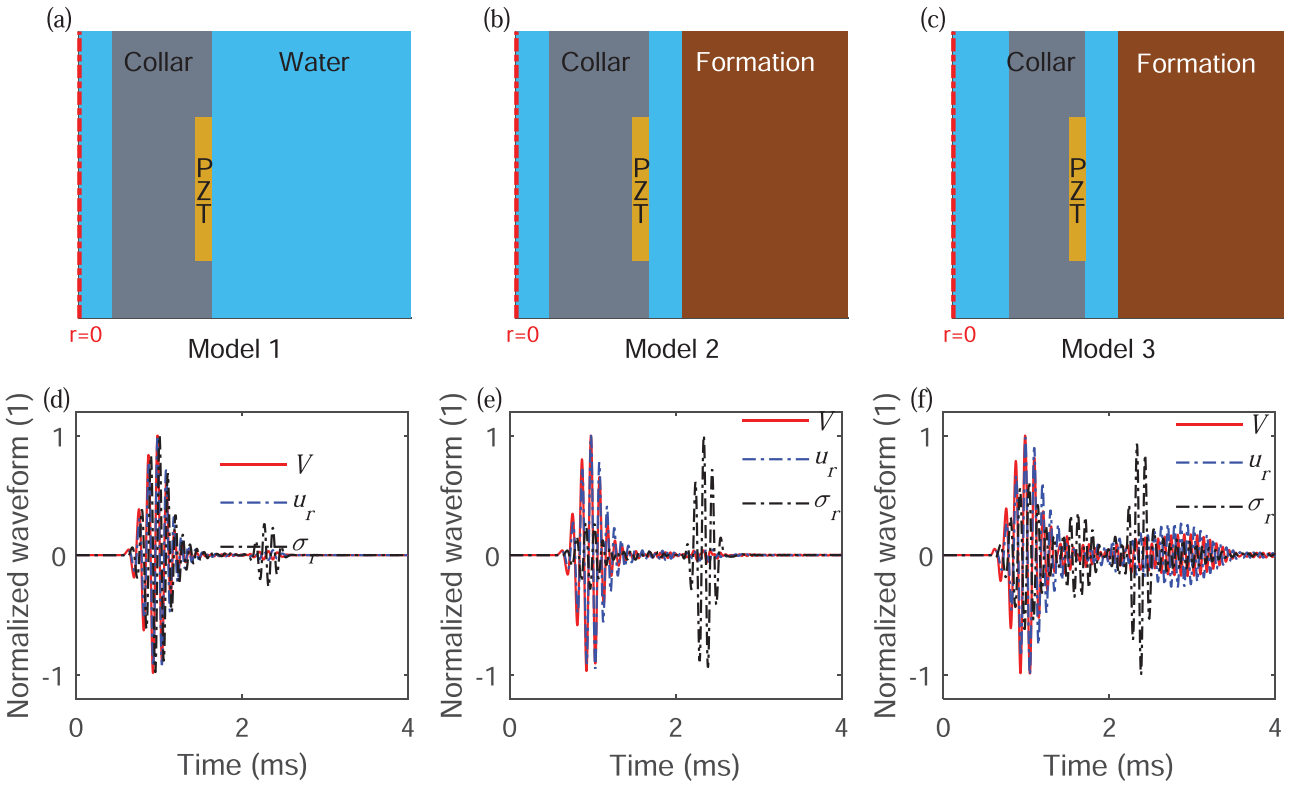

Figure 6. The schematics of the three models and the corresponding voltage, radial displacement and radial stress (negative pressure) waveforms. In (a) and (d), collars with a thickness of 0.063 m are placed in the infinite fluid; In (b) and (e), collars with a thickness of 0.063 m are placed in the infinite borehole. In (c) and (f), collars with a thickness of 0.050 m are placed in the borehole. The center frequency of the voltage source is 10 kHz.

Stoneley wave, which is also similar to the characteristic of voltage waveforms. However, the pressure waveform in figure 6e has a weak collar wave and a strong Stoneley wave, which is contrary to the characteristic of the voltage waveform. The comparison between figure 6d and e shows that the characteristic difference between voltage waveform and pressure waveform becomes larger when the formation exists, which is mainly reflected in the relative amplitude of collar wave. As in figure 6f, when the collar of thin is placed in the borehole, the characteristics of these three waveforms are similar to those in figure 6e. The comparison between figure 6e and f shows that the difference between voltage waveform and pressure waveform is still large when the collar becomes thinner, which is mainly reflected in the relative amplitude of the collar wave.

Most scholars present a weak collar wave and a strong Stongley wave in their simulated monopole acoustic LWD waveforms (Cui 2004; Wang *et al.* 2013; Su *et al.* 2015; Fang & Cheng 2017; Zheng 2017), which is consistent with the characteristics of pressure waveform described before. It seems that they assume pressure is recorded by the transducer. However, from the previous analysis, it can be seen that the normalised voltage waveform is very different from the normalised pressure waveform, mainly in the relative amplitudes of the drill collar wave and Stoneley wave.

3.2. *Similarity between various mechanical quantities and voltage signals*

The section 3.1 revealed that the voltage represents neither pressure nor radial displacement. In this section, we quantitatively compare the waveform of various mechanical quantities with the voltage waveform.

In different excitation frequencies, we calculate the waveforms of the voltage V, strain ε, stress σ, displacement $\mathbf{u}$, particle velocity $\mathbf{v}$ and particle acceleration $\mathbf{a}$ at the outer wall of the transducer. We compare the normalised waveforms of the above mechanical quantities with the normalised waveform of voltage, and measure their similarities using the Dynamic Time Warping method (Itakura 1975; Sakoe & Chiba 1978) as follows,

$$\mathrm{L}(\mathbf{A},\mathbf{B}) = \min_{F}\left[\frac{\sum_i d(\mathbf{A},\mathbf{B})\, w_i}{\sum_i w_i}\right], \tag{12}$$

where L is the time-normalised distance between two waveforms $\mathbf{A}$ and $\mathbf{B}$, that is, the difference between the two waveforms. The smaller the L value, the more similar waveform $\mathbf{A}$ and waveform $\mathbf{B}$ are, and the L value of zero means that $\mathbf{A}$ and $\mathbf{B}$ overlap. w_i is a nonnegative weighting coefficient; F is warping function and $d(\mathbf{A},\mathbf{B})$ is the minimum residual distance taking warping function F into account.

Figure 7 shows the comparisons of the normalised waveforms between mechanical quantities and voltage at the center frequency of 5 kHz. The gray lines represent the normalised voltage waveform, and the black dot lines represent the waveforms of the mechanical quantities marked on the left side of the frame. The subscripts r, z and θ indicate the radial, axial and circumferential components, respectively. It is worth noting that u_θ, v_θ and a_θ are zero in the monopole LWD, so they are not shown in figure 7. The L value represents the time-normalised distance between the normalised mechanical waveform and the normalised voltage waveform. It can be seen that the radial strain ε_r is most similar to the voltage, whereas the radial stress σ_r is least similar to the voltage.

The L values between these mechanical quantities waveforms and the voltage waveform at 5 kHz in figure 7 are sorted in the first row of Table 3, and the cases of 10 and 15 kHz are also shown in the other rows of Table 3. In addition, for the collar waves and the Stoneley waves obtained by adding a rectangular window to the full wave, we also calculate the L values between various mechanical quantities waveforms and voltage waveforms. In each row of Table 3, the mechanical quantities are sorted according to the corresponding L values (in parenthesis) from small to large, that is, according to the corresponding similarities from strong to weak.

This similarity sorting varies with frequencies and the wave types. In Table 3, all the L values are nonzero, which means that none of the mechanical waveform overlaps the voltage waveform. Thus, the voltage recorded by the transducer is not contributed by a single mechanical quantity, but is more likely to be contributed by a combination of several mechanical quantities.

3.3. *Relation between four mechanical quantities and voltage*

In section 3.2, it was shown that voltage is more likely to be converted from a combination of several mechanical quantities rather than a single mechanical quantity. What mechanical quantities are converted into voltage? What is the weight of each mechanical quantity? In this section, the piezoelectric equations (Safari & Akdogan 2008) are introduced to explore the answer, as

$$\begin{cases} \varepsilon_\theta = s_{11}^E\sigma_\theta + s_{12}^E\sigma_z + s_{13}^E\sigma_r + d_{31}E_r \\ \varepsilon_z = s_{12}^E\sigma_\theta + s_{11}^E\sigma_z + s_{13}^E\sigma_r + d_{31}E_r \\ \varepsilon_r = s_{13}^E\sigma_\theta + s_{13}^E\sigma_z + s_{33}^E\sigma_r + d_{33}E_r \end{cases}, \tag{13}$$

where $s_{1i}, i = 1, 2, 3$, $d_{3j}, j = 1, 2, 3$ illustrate compliance coefficient and piezoelectric constant of the piezoelectric ceramic tube respectively, as shown in Table 2; E_r is the radial electric field intensity. The subscripts 1, 2 and 3 indicate the circumferential, axial and radial components, respectively.

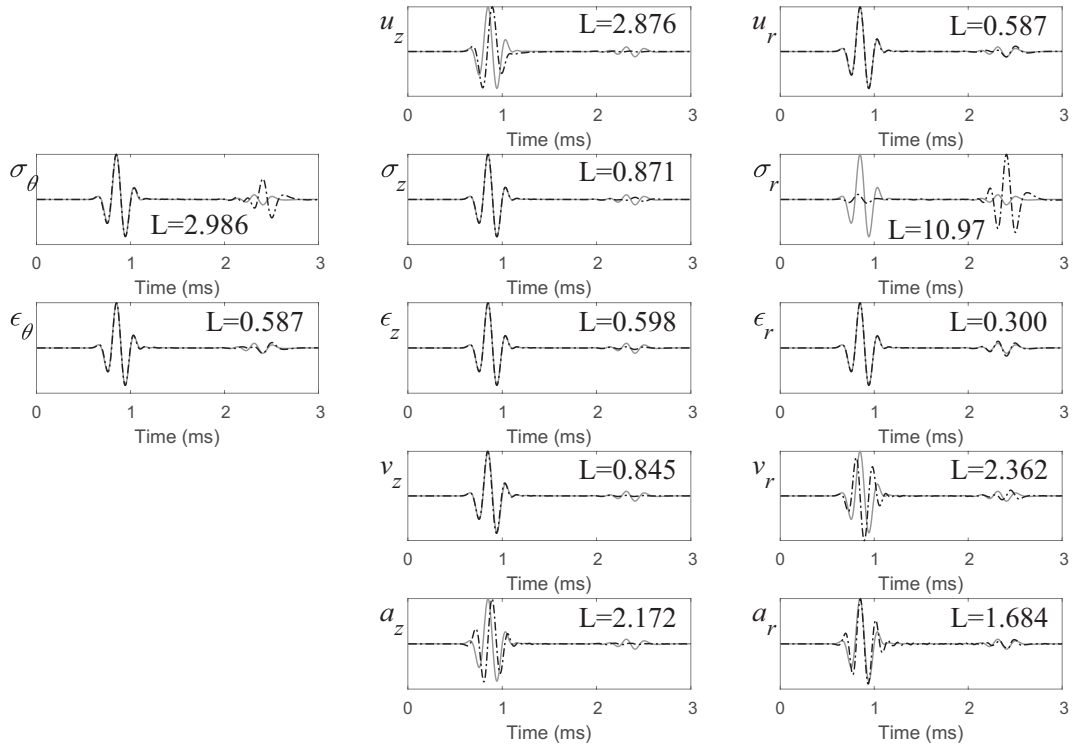

Figure 7. Comparisons of the normalised waveforms between the mechanical quantities and the voltage at the center frequency of 5 kHz. The gray line represents the normalised voltage waveform, and the black dot line represents the waveforms of the mechanical quantities marked on the left side of the frame.

For a radially polarised thin tube piezoelectric transducer (Fa *et al.* 1996),

$$V = \delta E_r, \tag{14}$$

$$\varepsilon_\theta = \frac{u_r}{r}, \tag{15}$$

where δ is the thickness of the piezoelectric ceramic and r represents the distance from the outer wall of the transducer to the borehole axis.

Thus, the voltage V can be formulated in terms of the four arbitrary mechanical quantities among u_r, σ_r, ε_r, σ_z, ε_z and σ_θ. It is worth noting that piezoelectric ceramics are the research object of piezoelectric equations, so these mechanical quantities are of the piezoelectric ceramics in the transducer. But it is the mechanical quantity of the borehole fluid that is expected to be sensed by the transducer in acoustic LWD. According to the boundary conditions in equation (10), radial displacement u_r and radial stress σ_r are continuous between the transducer and the borehole fluid. That is to say, u_r and σ_r are also the mechanical quantities of the borehole fluid. Therefore, when choosing the four from the six quantities to represent V, u_r and σ_r, as the mechanical quantities of the borehole fluid, these should be the candidates. Besides, from the Table 3 the radial strain ε_r and axial stress σ_z have shown high similarities to voltage, which also be the better candidates. To sum up, u_r, σ_r, ε_r, and σ_z are combined to represent the voltage which can be obtained by substituting equations (13) and (15) into equation (14), as

$$V = V_1 + V_2 + V_3 + V_4, \tag{16}$$

with

$$V_1 = \frac{s_{13}\delta}{r\left(s_{13}d_{31} - s_{11}d_{33}\right)}u_r, \tag{17a}$$

$$V_2 = -\frac{\left(s_{13}^{\ 2} - s_{11}s_{33}\right)\delta}{s_{13}d_{31} - s_{11}d_{33}}\sigma_r, \tag{17b}$$

$$V_3 = -\frac{s_{11}\delta}{\left(s_{13}d_{31} - s_{11}d_{33}\right)}\varepsilon_r, \tag{17c}$$

$$V_4 = -\frac{s_{13}\left(s_{12} - s_{11}\right)\delta}{s_{13}d_{31} - s_{11}d_{33}}\sigma_z. \tag{17d}$$

The first two voltage components in equation (16) are derived from the weighted mechanical quantities of the borehole fluid, which reflect the borehole fluid and formation information. The last two voltage components in equation (16) are derived from the weighted mechanical quantities of the transducer, which reflect the interference of the measurement tool to the borehole information. When measuring formation information of interest to scholars, the interference of the measurement tools on results needs to be

Table 3. Similarities sorting between various mechanical quantities (strain, stress, displacement, particle velocity and particle acceleration) waveforms and voltage waveforms in different frequencies. In each row, the mechanical quantities are sorted according to the corresponding L values (in parenthesis) from small to large

Center frequency	Wave type	Mechanical quantities											
5 kHz	Full wave	ε_r	u_r	ε_θ	ε_z	v_z	σ_z	a_r	a_z	v_r	u_z	σ_θ	σ_r
		(1)	(m)	(1)	(1)	(m s^{-1})	(N m^{-2})	(m s^{-2})	(m s^{-2})	(m s^{-1})	(m)	(N m^{-2})	(N m^{-2})
		(0.300)	(0.587)	(0.587)	(0.598)	(0.845)	(0.871)	(1.684)	(2.172)	(2.362)	(2.876)	(2.986)	(10.97)
	Collar wave	ε_r	σ_z	ε_z	σ_θ	v_z	u_r	ε_θ	σ_r	a_r	a_z	v_r	u_z
		(1)	(N m^{-2})	(1)	(N m^{-2})	(m s^{-1})	(m)	(1)	(N m^{-2})	(m s^{-2})	(m s^{-2})	(m s^{-1})	(m)
		(0.202)	(0.262)	(0.455)	(0.547)	(0.686)	(0.695)	(0.695)	(1.372)	(4.958)	(5.486)	(6.594)	(7.892)
	Stoneley wave	ε_r	σ_r	ε_z	v_r	a_r	σ_θ	u_r	ε_θ	σ_z	v_z	a_z	u_z
		(1)	(N m^{-2})	(1)	(m s^{-1})	(m s^{-2})	(N m^{-2})	(m)	(1)	(N m^{-2})	(m s^{-1})	(m s^{-2})	(m)
		(0.942)	(4.452)	(4.615)	(6.206)	(6.855)	(8.013)	(9.781)	(9.781)	(11.70)	(13.87)	(19.26)	(19.81)
10 kHz	Full wave	ε_z	σ_z	v_z	u_z	ε_r	u_r	ε_θ	a_z	a_r	v_r	σ_θ	σ_r
		(1)	(N m^{-2})	(m s^{-1})	(m)	(1)	(m)	(1)	(m s^{-2})	(m s^{-2})	(m s^{-1})	(N m^{-2})	(N m^{-2})
		(0.713)	(0.922)	(1.111)	(1.148)	(1.264)	(1.477)	(1.477)	(1.789)	(2.965)	(3.618)	(9.675)	(12.53)
	Collar wave	ε_r	σ_z	ε_z	u_z	v_z	u_r	ε_θ	a_z	a_r	σ_r	v_r	σ_θ
		(1)	(N m^{-2})	(1)	(m)	(m s^{-1})	(m)	(1)	(m s^{-2})	(m s^{-2})	(N m^{-2})	(m s^{-1})	(N m^{-2})
		(0.278)	(0.507)	(0.796)	(1.198)	(1.253)	(1.912)	(1.912)	(2.405)	(4.038)	(5.537)	(5.801)	(6.918)
	Stoneley wave	ε_r	ε_z	σ_r	σ_z	σ_θ	u_r	ε_θ	v_r	a_r	v_z	a_z	u_z
		(1)	(1)	(N m^{-2})	(N m^{-2})	(N m^{-2})	(m)	(1)	(m s^{-1})	(m s^{-2})	(m s^{-1})	(m s^{-2})	(m)
		(3.042)	(4.736)	(4.768)	(5.966)	(6.968)	(9.069)	(9.069)	(10.07)	(10.28)	(26.93)	(31.13)	(36.87)
15 kHz	Full wave	σ_z	ε_r	v_z	ε_z	a_z	u_z	σ_θ	a_r	v_r	σ_r	u_r	ε_θ
		(N m^{-2})	(1)	(m s^{-1})	(1)	(m s^{-2})	(m)	(N m^{-2})	(m s^{-2})	(m s^{-1})	(N m^{-2})	(m)	(1)
		(1.506)	(1.512)	(2.431)	(4.370)	(4.413)	(4.896)	(6.540)	(9.305)	(11.24)	(20.33)	(26.98)	(26.98)
	Collar wave	σ_z	ε_z	ε_r	σ_θ	v_z	a_z	u_z	σ_r	v_r	u_r	ε_θ	a_r
		(N m^{-2})	(1)	(1)	(N m^{-2})	(m s^{-1})	(m s^{-2})	(m)	(N m^{-2})	(m s^{-1})	(m)	(1)	(m s^{-2})
		(0.737)	(1.132)	(1.189)	(1.974)	(2.058)	(4.956)	(10.95)	(11.27)	(12.48)	(12.55)	(12.55)	(14.39)
	Stoneley wave	v_z	σ_z	ε_z	u_r	ε_θ	σ_θ	a_r	ε_r	v_r	u_z	a_z	σ_r
		(m s^{-1})	(N m^{-2})	(1)	(m)	(1)	(N m^{-2})	(m s^{-2})	(1)	(m s^{-1})	(m)	(m s^{-2})	(N m^{-2})
		(2.716)	(2.892)	(5.200)	(6.077)	(6.077)	(6.365)	(6.552)	(9.002)	(9.832)	(13.39)	(16.11)	(18.21)

minimised. Therefore, to highlight the formation information, we can increase the weighting of the former two and meanwhile reduce the weighting of the latter two in equation (16) by adjusting the material and size of the transducer tool. This is worth investigating but is not the main topic of this paper. So far, we have answered the question posed at the beginning of this section.

The voltage components contributed by u_r, σ_r, ε_r and σ_z are expressed in equation (17) and their waveforms at different center frequencies are shown in figure 8. The mechanical quantities are calculated by the FEM-PP. The black dot lines represent the voltage components V_1, V_2, V_3 and V_4 contributed by u_r, σ_r, ε_r and σ_z, respectively. The blue dashed lines represent the sum of the four voltage components. The red lines represent the voltage V recorded by the transducer.

From the top waveforms at different frequencies in figure 8, the waveform of voltage V is almost identical to the waveform superimposed by the four voltage components, which is consistent with equation (16). By comparing the amplitude between the waveforms of voltage V and the four voltage components, it can be seen that u_r, ε_r and σ_z contribute a lot to the collar wave, and can be used as the major targets in the study of the properties of collar waves. On the other hand, σ_r makes little contribution to the collar wave but a great contribution to the Stoneley wave, which may be helpful in the study of inversing formation permeability by using Stoneley waves.

3.4. *Influence of collar grooving on the waveform of various mechanical quantities*

These analyses are based on a smooth drill collar. Considering that the drill collar is usually grooved in actual logging, we study the waveforms of various mechanical quantities under two grooving cases in this section. Figure 9 parts a and b show the schematic of the interior and exterior grooved drill collars, respectively, in which the groove number is 10; $D = 0.021m$; $W = 0.12m$ and $S = 0.12m$ (Yang *et al.* 2017). Figure 9c shows the waveforms of voltage, radial displacement and pressure under different grooving cases, in which the solid red lines represent the waveforms of a smooth drill collar, and the dashed black and blue lines represent the waveforms after interior and exterior grooving, respectively.

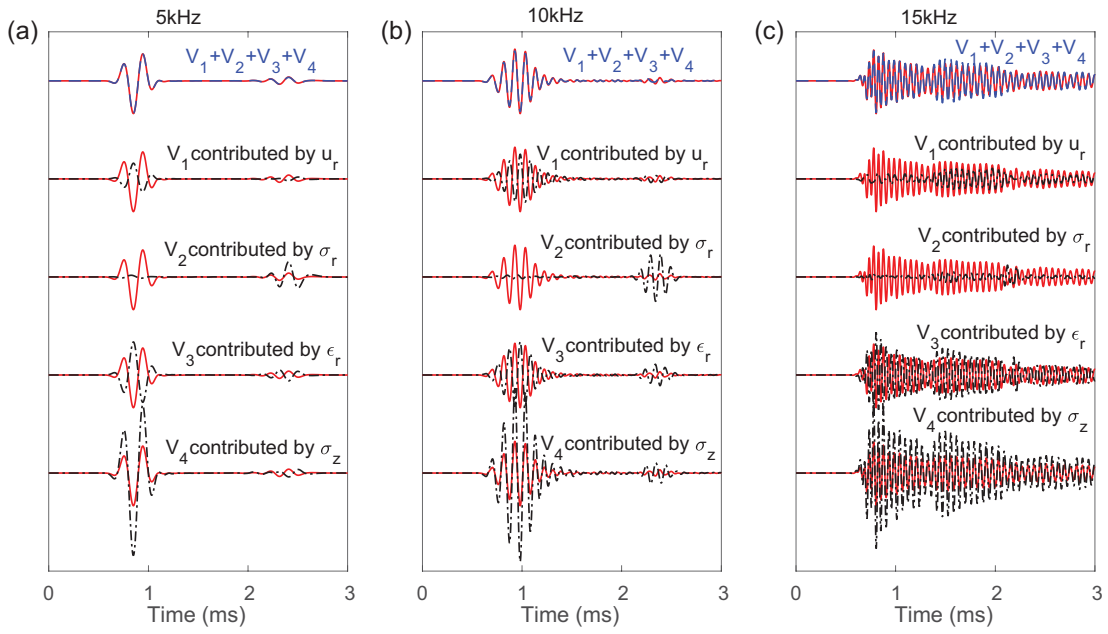

Figure 8. The contributions of u_r, σ_r, σ_z and ε_r to V at different center frequencies (a) 5 kHz, (b) 10 kHz and (c) 15 kHz. The black dotted lines represent the voltage components V_1, V_2, V_3 and V_4, which, respectively, contributed to u_r, σ_r, ε_r and σ_z. The blue dashed lines represent the sum of the four voltage components. The red lines represent voltage V recorded by the transducer.

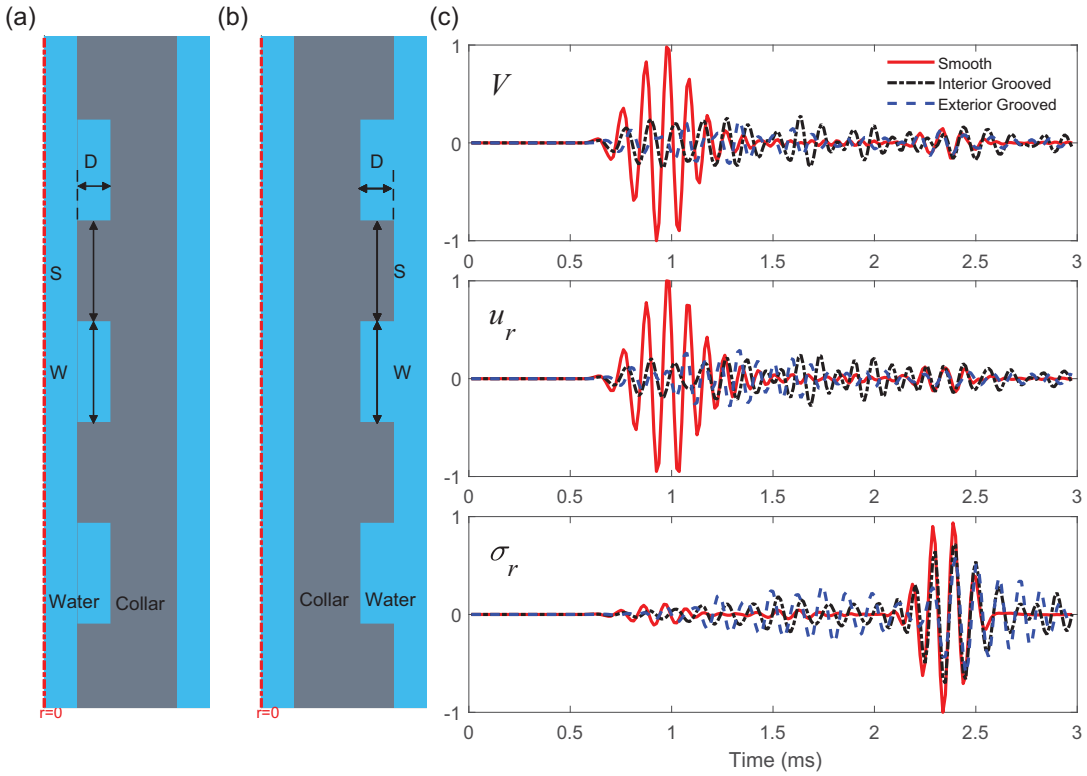

Figure 9. Schematics of the (a) interior grooved collar and (b) exterior grooved collar. (c) Waveforms of voltage, radial displacement and pressure with smooth collar, interior grooved collar and exterior grooved collar. The solid red lines represent the waveforms of a smooth drill collar, and the dashed black and blue lines represent the waveforms after interior and exterior grooving, respectively. The drill collars in (a) and (b) both have ten grooves.

Compared with the case of smooth collar, the collar wave of each mechanical quantity after grooving, regardless of the interior and exterior groove, exhibits the characteristics of amplitude decreasing and duration increasing. Compared with pressure waveform, the effect of grooving on radial displacement waveform is more similar to the voltage waveform. This indicates that the displacement waveform before and after grooving should also be displayed when measuring the grooving effect instead of only the pressure waveform as in previous studies (Yang 2019).

4. Conclusions

By the proposed FEM-PP method considering both the piezoelectric effect of the transducer and the propagation of the acoustic wave, we simulated the mechanical responses and output voltage in monopole acoustic LWD. The main conclusions included the following:

(i) The output voltage does not reflect the pressure in the borehole. The difference in their waveforms is that the voltage waveform contains a strong collar wave and a weak Stoneley wave, whereas the pressure waveform contains a weak collar wave and a strong Stoneley wave.
(ii) The output voltage recorded by the transducer is contributed to by a combination of multiple mechanical quantities rather than a single mechanical quantity. The combination includes the radial displacement and radial stress of the borehole fluid, which reflect the formation information, and the radial strain and axial stress of the transducer, which reflect the interference of the measuring tool. This reveals that the first two mechanical quantities should be given more weight when designing the receiver to highlight the formation information of interest.
(iii) The amplitudes of the waveforms are compared between the voltage and the four voltage components contributed by the four mechanical quantities. The results show that the radial displacement, radial strain and axial stress contribute a lot to the collar wave, whereas the radial stress contributes a lot to the Stoneley wave.
(iv) Grooving does not affect these analyses. The displacement waveform before and after grooving should also be displayed instead of only the pressure waveform as in previous studies when evaluating the grooving effect.

Acknowledgements

This work is jointly supported by National Natural Science Foundation of China (grant nos. 11972132 and 11734017).

Conflict of interest statement: None declared.

References

Birchak, J.R., Linyaev, E., Robbins, C.A. & Roessler, D.E., 1997. Acoustic transducer for LWD tool, *U.S. Patent* 5,644,186.

Cui, Z.W., 2004. *Theoretical and numerical study of modified Biot's models, acoustoelectric well logging and acoustic logging while drilling excited by multipole acoustic sources, PhD. dissertation,* Jilin University.

Fa, L., Lin, F. & Chen, W.H., 1996. Source function derivation and property analysis of ceramic ring transducer for petroleum exploration, *Chinese Journal of Geophysics*, **S1**, 387–399 (in Chinese).

Fang, X.D. & Cheng, A., 2017. Detection of formation S-wave in a slow formation using a monopole acoustic logging-while-drilling tool, *Geophysics*, **83**, D9–D16.

Givoli, D. & Neta, B., 2004. High-order Non-reflecting boundary scheme for time-dependent waves, *Journal of Computational Physics*, **86**, 24–46.

He, X., Wang, X. & Chen, H., 2017. Theoretical simulations of wave field variation excited by a monopole within collar for acoustic logging while drilling, *Wave Motion*, **72**, 287–302.

Itakura, F., 1975. Minimum prediction residual principle applied to speech recognition, *IEEE Transactions on Acoustics, Speech, and Signal Processing*, **23**, 67–72.

Ji, Y., He, X., Chen, H., Wang, X. & Zhang, H., 2019. Monopole collar wave characteristics for acoustic logging while drilling in fast formations in the frequency and spatial domains, *Wave Motion*, **90**, 66–81.

Lalanne, B. & Touratier, M., 2000. Aeroelastic vibrations and stability in cyclic symmetric domains, *International Journal of Rotating Machinery*, **6**, 445–452.

Matuszyk, P.J. & Torres-Verdín, C., 2014. Frequency-domain simulation of logging-while-drilling borehole sonic waveforms, *Geophysics,* **79**, D99–D113.

Safari A. & Akdogan E.K., eds, 2008. *Piezoelectric and Acoustic Materials for Transducer Applications*, Springer Science & Business Media.

Sakoe, H. & Chiba, S., 1978. Dynamic programming algorithm optimization for spoken word recognition, *IEEE Transactions on Acoustics, Speech, and Signal Processing*, **26**, 43–49.

Sinha, B.K., Şimşek, E. & Asvadurov, S., 2009. Influence of a pipe tool on borehole modes, *Geophysics,* **74**, E111–E123.

Su, Y., Tang, X., Xu, S. & Zhang, C., 2015. Acoustic isolation of a monopole logging while drilling tool by combining natural stopbands of pipe extensional waves, *Geophysical Journal International,* **202**, 439–445.

Tang, X.M., Dubinsky, V. & Wang, T., 2002. Shear-velocity measurement in the logging-while-drilling environment: modeling and field evaluations, *43rd SPWLA Annul. Logging* Symposium.

Wang, H., Fehler, M., Tao, G. & Wei, Z., 2016. Investigation of collar properties on data-acquisition scheme for acoustic logging-while-drilling, *Geophysics,* **81**, D611–D624.

Wang,, H., Tao, G. & Zhang, K., 2013. Borehole acoustic reflection logging by FDM and FEM simulations and data analysis, *2013 SEG Annual Meeting, Expanded Abstracts,* 621–625.

Wang, J., Hu, H., Guan, W., Li, H., Zheng, X. & Yang, Y., 2017. Electrokinetic measurements of formation velocities with wireline seismoelectric logging and seismoelectric logging while drilling: *Chinese Journal of Geophysics (in Chinese),* **60**, 862–872.

Wang, J., Zhu, Z.Y. & Zheng, X.B., 2016. Experimental analysis on acoustic LWD with multipole source: *Chinese Journal of Geophysics (in Chinese),* **59**, 1909–1919.

Wisniewski, L., Varsamis, G.L. & Mandal, B., 2003. Acoustic logging tool having programmable source waveforms, *U.S. Patent* 6,661,737.

Yang, Y., Guan, W., Hu, H. & Xu., M., 2017. Numerical study of the collar wave characteristics and the effects of grooves in acoustic

logging while drilling, *Geophysical Journal International*, **209**, 749–761.

Yang, Y. F., 2019. *Three-dimensional finite difference simulation of acoustic logging while drilling and study on acoustic insulation performance of grooved drill collar*, *PhD. dissertation*, Harbin Institute of Technology.

Zhang, B., Dong, H. & Wang, K., 1994. Multipole sources in a fluid-filled borehole surrounded by a transversely isotropic elastic solid, *The Journal of the Acoustical Society of America*, **96**, 2546–2555.

Zheng, X. B., 2017. *Theoretical simulations of monopole and dipole acoustic logging while drilling and investigations of propagation mechanism for individual waves*, *PhD. dissertation*, Harbin Institute of Technology.

Zhu, Z., Toksöz, M.N., Rao, R. & Burns, D. R., 2008. Experimental studies of monopole, dipole, and quadrupole acoustic logging while drilling (LWD) with scaled borehole models, *Geophysics,* **73**, E133–E143.